LETTERS

Capture of hydroxymethylene and its fast disappearance through tunnelling

Peter R. Schreiner[1], Hans Peter Reisenauer[1], Frank C. Pickard IV[2], Andrew C. Simmonett[2], Wesley D. Allen[2], Edit Mátyus[3] & Attila G. Császár[3]

Singlet carbenes exhibit a divalent carbon atom whose valence shell contains only six electrons, four involved in bonding to two other atoms and the remaining two forming a non-bonding electron pair. These features render singlet carbenes so reactive that they were long considered too short-lived for isolation and direct characterization. This view changed when it was found that attaching the divalent carbon atom to substituents that are bulky and/or able to donate electrons produces carbenes that can be isolated and stored[1]. *N*-heterocyclic carbenes are such compounds now in wide use, for example as ligands in metathesis catalysis[2]. In contrast, oxygen-donor-substituted carbenes are inherently less stable and have been less studied. The pre-eminent case is hydroxymethylene, H–C–OH; although it is the key intermediate in the high-energy chemistry of its tautomer formaldehyde[3–7], has been implicated since 1921 in the photocatalytic formation of carbohydrates[8], and is the parent of alkoxycarbenes that lie at the heart of transition-metal carbene chemistry, all attempts to observe this species or other alkoxycarbenes have failed[9]. However, theoretical considerations indicate that hydroxymethylene should be isolatable[10]. Here we report the synthesis of hydroxymethylene and its capture by matrix isolation. We unexpectedly find that H–C–OH rearranges to formaldehyde with a half-life of only 2 h at 11 K by pure hydrogen tunnelling through a large energy barrier in excess of 30 kcal mol^{-1}.

Apart from Fischer carbenes—named after the chemist who prepared the first metal-carbene compound, $W(CO)_5(C(CH_3)OCH_3)$ (ref. 11)—oxygen-donor-substituted carbenes have received little attention, mostly because of the lack of suitable synthetic precursors. Even the tetra-atomic hydroxymethylene archetype (**1**; Fig. 1) has not been isolated until now because the starting materials necessary for typical carbene generation strategies are too unstable or too difficult to prepare.

We devised a route to **1** using thermal extrusion of CO_2 (refs 12, 13) from glyoxylic acid (**3**; Fig. 1) via high-vacuum flash pyrolysis (HVFP), followed by immediate matrix isolation. This approach is probably of general utility for generating otherwise inaccessible carbenes. Starting material **3** is a commodity that can be readily purified
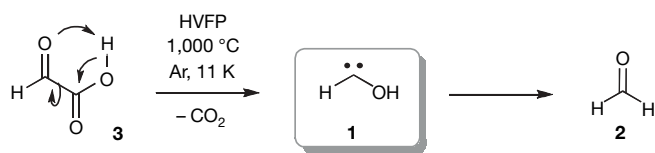
for matrix isolation experiments. It is also volatile enough to enable vaporization and transport through a heated quartz tube. After several attempts and optimization of the reaction parameters (temperature, gas flow, length and diameter of quartz tube), we were successful in the generation and trapping of **1** in an argon matrix at 11 K (see Methods for details).

We characterized H–C–OH and H–C–OD by measuring their infrared spectra (Fig. 2a, b) and comparing them with decisive electronic structure and variational nuclear motion computations, the latter using a high-quality quartic vibrational force field. Inspection of Table 1 shows remarkable agreement between measured and predicted vibrational band origins (VBOs), which provides convincing evidence for the successful preparation of **1**. For 13 of the 15 assigned bands of *trans*-H–C–OH and *trans*-H–C–OD, the mean and standard deviation of the residual between theory and experiment are only 6.0 and 3.3 cm^{-1}, respectively, which is well within the expected range of matrix shifts. We stress that no empirical adjustments were applied to the variationally computed VBOs. The related harmonic frequencies also displayed in Table 1 demonstrate that the full inclusion of vibrational anharmonicity is essential for achieving such a high level of agreement. Particularly impressive is the match for four combination and overtone levels: $v_3 + v_4$ of H–C–OH, $2v_3$ of H–C–OD, and the Fermi resonance pair $(v_3 + v_4, v_1)$ of H–C–OD. The only notable disparities in Table 1 occur for v_1(OH stretch) of **1** and v_2(OD stretch) of $[D_1]$-**1**, for which the experimental assignments lie 61 and 39 cm^{-1}, respectively, below the theoretical values. Matrix shifts of this magnitude for vibrational fundamentals are not unprecedented[14].

The recorded ultraviolet/visible spectrum of **1** displays one very weak absorption band between 500 and 380 nm (wavelength of maximum absorption, 427 nm) with a distinctive vibrational fine structure (Fig. 3). Irradiation of the matrix with monochromatic light within this spectral range (435, 470 and 500 nm) causes rapid rearrangement of **1** to formaldehyde (**2**; Fig. 1) and partial fragmentation into CO and H_2. On the basis of rigorous multireference coupled cluster computations within the Mk-MRCCSD formalism[15], we attribute the signals in Fig. 3 to the lowest-lying open-shell singlet excited electronic state (S_1) of carbene **1**. Upon geometry optimization, the S_1 state of **1** relaxes to a non-planar structure with a widened H–C–O angle of 127.4° and a dihedral angle of 108.4°, consistent with the extensive vibrational progression observed in the electronic absorption spectrum. Our best theoretical vertical and adiabatic excitation energies are 2.99 eV (415 nm) and 2.40 eV (516 nm), respectively, in complete accord with experiment.

For further theoretical characterization of **1**, we optimized all singlet structures related to **1** at the rigorous AE-CCSD(T)/cc-pCVQZ

Figure 1 | Generation of hydroxymethylene (1). Thermal extrusion of CO_2 through high-vacuum flash pyrolysis (HVFP) from glyoxylic acid (**3**) and rearrangement of **1** to formaldehyde (**2**).

[1]Institut für Organische Chemie der Justus-Liebig-Universität, Heinrich-Buff-Ring 58, D-35392 Giessen, Germany. [2]Center for Computational Chemistry and Department of Chemistry, University of Georgia, Athens, Georgia 30602, USA. [3]Laboratory of Molecular Spectroscopy, Institute of Chemistry, Eötvös University, H-1518 Budapest 112, PO Box 32, Hungary.
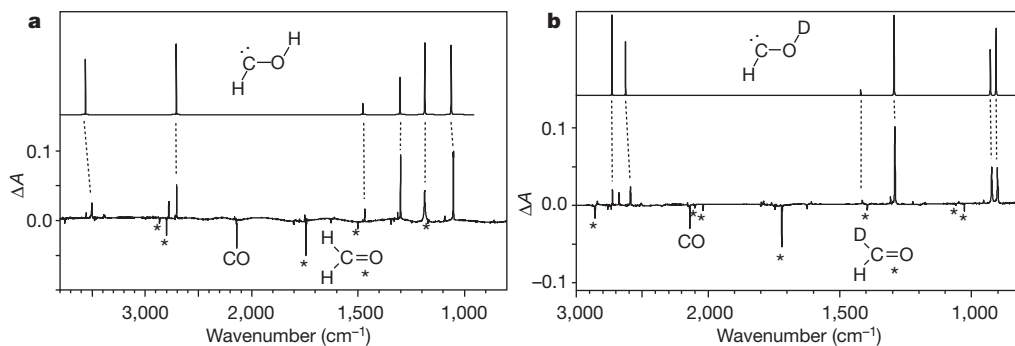
Figure 2 | Infrared spectra of 1 and [D₁]-1. a, Lower trace, hydroxymethylene (Ar matrix, 11 K) difference infrared spectrum (absorbance change ΔA) obtained by subtracting the spectra of unirradiated and irradiated (2 min at 470 nm) matrix-isolated pyrolysis products of glyoxylic acid. Upper trace, computed AE-CCSD(T)/cc-pCVQZ variational anharmonic VBOs of *trans*-hydroxymethylene (**1t**) and double-harmonic intensities from Table 1. Asterisks indicate peaks assigned to **2**. **b**, Lower trace, [D₁]-hydroxymethylene (Ar matrix, 11 K) difference infrared spectrum obtained by subtracting the spectra of unirradiated and irradiated (2 min at 470 nm) matrix-isolated pyrolysis products of [D₁]-glyoxylic acid. Upper trace, computed AE-CCSD(T)/cc-pCVQZ variational anharmonic VBOs of [D₁]-*trans*-hydroxymethylene and double-harmonic intensities from Table 1.

level and pinpointed their relative energies to around 0.1 kcal mol⁻¹ by means of exhaustive focal-point analyses (FPA)[16]. (For structural depictions, optimized *xyz* coordinates, and FPA energetic tables, see Supplementary Figs 1 and 2, Supplementary Tables 2 and 3, and Supplementary Tables 4–10, respectively; for full details of the theoretical approach, see Methods.) The potential energy surface[17] surrounding **1** is shown schematically in Fig. 4. Hydroxymethylene exhibits a *trans*-planar equilibrium structure (**1t**) with an H–C–O angle of 102.3°. The C–O bond length of 1.311 Å is much shorter than the corresponding 1.427 Å distance in methanol[18], indicative of the expected π-type stabilization of the electron-deficient carbene centre through the adjacent oxygen *p* lone pair. Our FPA computations place the lowest triplet state of H–C–OH much higher in energy ($T_0 = 28.0$ kcal mol⁻¹) than the closed-shell singlet **1t**. This large separation increases at the transition state (**TS2**; Fig. 4) for isomerization

to formaldehyde, where AE-CCSD(T)/cc-pCVQZ theory gives a singlet–triplet energy difference of 37.6 kcal mol⁻¹. These results indicate that intersystem crossing to triplet surfaces should not occur in our experiments. In addition, we find no evidence for the *cis*-**1** isomer (**1c**; Fig. 4) that lies 4.4 kcal mol⁻¹ above **1t**, presumably because of the high barrier (**TS1**, 26.8 kcal mol⁻¹; Fig. 4) for internal rotation and because the CO_2 extrusion process of Fig. 1 is likely to yield exclusively **1t** (similar processes yielding only specific conformers have been reported before[19]). The barrier computed for the rearrangement of **1t** to **2** is even higher (**TS2**, 29.7 kcal mol⁻¹), which reinforces the earlier theoretical prediction[10] that hydroxymethylene should be observable under matrix isolation conditions.

Despite being located at an energy minimum on the potential energy surface that is surrounded by high enthalpic barriers, matrix-isolated **1** disappears quickly with a half-life ($t_{1/2}$) of ~2 h in Ar, Kr and Xe matrices. The magnitude of $t_{1/2}$ is virtually independent of temperature in the 11–20 K range (see Supplementary Table 1). In contrast, the monodeuterated species ([D₁]-**1**) is completely stable under the same conditions. Thermal rearrangement through either **TS1** or **TS2** is not conceivable at such low temperatures. Because of the low concentration of **1**, the very limited mobility of molecules in noble-gas matrices, and the observed lack of temperature dependence of $t_{1/2}$, bimolecular reactions are also an unlikely cause. Therefore, quantum mechanical tunnelling appears to be the most viable mechanism behind the rapid disappearance of *trans*-H–C–OH as well as the persistence of H–C–OD. It is relevant that strong tunnelling effects in unimolecular reactions on the potential energy

Table 1 | Comparison of computed and experimental vibrational frequencies

Vibrational description*	ω (I_{rel})	ν	Expt. (I_{rel})
***trans*-H–C–OH (1t)**			
78% v_1(OH str.) + 8% [$v_3 + 2v_6$]	3,765.4 (57)	3,561.6	3,500.6 (43)
84% [$v_4 + v_5 + v_6$]		3,520.8	
83% [$3v_5$]		3,516.0	
72% [$v_3 + v_4$] + 15% v_2(CH str.) + 14% [$v_3 + v_5$]		2,785.5	2,776.2 (16)
55% v_2(CH str.) + 18% [$v_3 + v_4$]	2,876.6 (99)	2,706.5	2,703.3 (37)
96% v_3(HOC def. + HCO def.)	1,513.7 (13)	1,475.1	1,465.5 (10)
92% v_4(CO str.)	1,334.1 (39)	1,300.5	1,297.1 (53)
97% v_5(HOC def. − HCO def.)	1,220.0 (100)†	1,183.5	1,183.2 (100)
97% v_6(twist)	1,094.3 (82)	1,058.9	1,048.5 (88)
***trans*-H–C–OD ([D₁]-1t)**			
87% [$2v_3$] + 7% v_1		2,852.6	2,841.3 (8)
51% [$v_3 + v_4$] + 33% v_1(CH str.) + 5% [$2v_3$]	2,878.9 (100)‡	2,729.5	2,726.1 (30)
45% v_1(CH str.) + 37% [$v_3 + v_4$] + 5% v_2		2,682.8	2,675.9 (20)
83% v_2(OD str.)	2,739.5 (57)	2,626.8	2,588.1 (58)
78% [$2v_4$] + 5% v_4		2,566.4	
97% v_3(HCO def.)	1,451.0 (8)	1,420.8	1,414.7 (4)
92% v_4(CO str.)	1,326.4 (84)	1,294.1	1,290.8 (100)
98% v_5(DOC def.)	953.6 (58)	928.7	923.1 (66)
98% v_6(twist)	933.8 (70)	907.1	901.6 (59)

Theoretical (AE-CCSD(T)/cc-pCVQZ) harmonic (ω) and variational anharmonic (ν) vibrational band origins (in cm⁻¹) relative to experimental bands (Ar matrix, 11 K) for *trans*-hydroxymethylene and its monodeuterated isotopologue. Relative infrared absorption intensities (I_{rel}, in %) from the double-harmonic approximation are included from AE-CCSD(T)/cc-pVTZ computations.
* Distribution of the converged vibrational wavefunctions over the normal mode basis states; all contributions larger than 5% are listed.
† Absolute intensity, 142 km mol⁻¹.
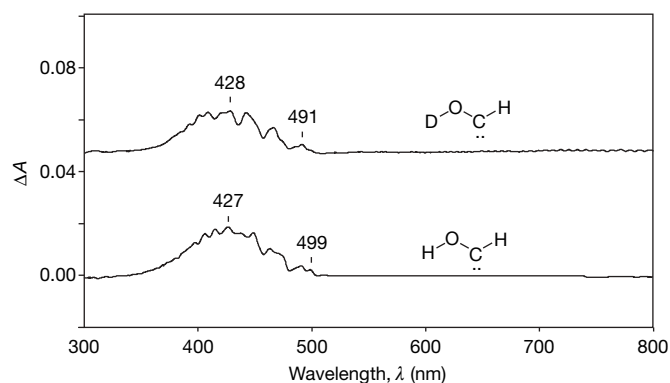‡ Absolute intensity, 116 km mol⁻¹.

Figure 3 | Ultraviolet/visible spectrum of 1 and [D₁]-1. Shown are difference ultraviolet/visible spectra (unirradiated − irradiated) of **1** and [D₁]-**1** in an argon matrix at 11 K.
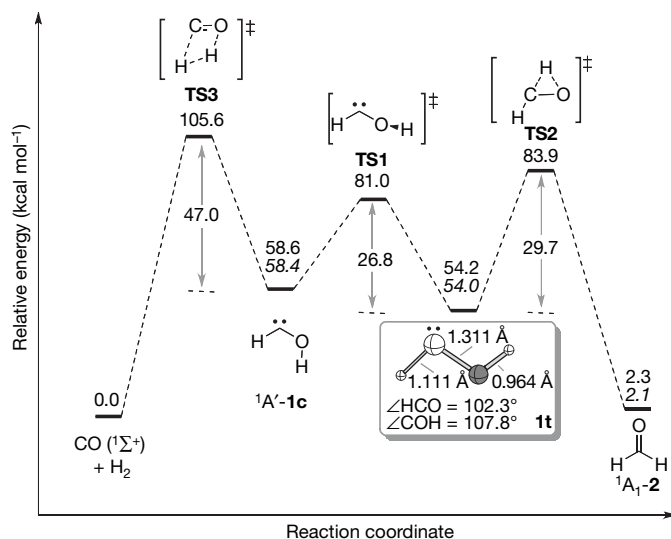
Figure 4 | Schematic H–C–O–H potential energy hypersurface. Key features of the computed energy profile (high-level coupled cluster focal point analyses + harmonic zero-point vibrational energies (ZVPE); values in italics use anharmonic ZPVEs) for the rearrangement of singlet **1** (**1c**, *cis* form; **1t**, *trans* form, inset) to formaldehyde and CO + H_2.

surface shown in Fig. 4 have been noted in a number of previous experimental and theoretical studies[20,21].

To obtain a theoretical tunnelling rate for **1t** isomerizing to **2**, we used the AE-CCSD/cc-pCVTZ method to precisely map out the intrinsic reaction path (IRP) connecting **TS2** to the reactant and product and to determine harmonic vibrational frequencies along this steepest-descent route. A final potential energy curve for the isomerization IRP was then constructed from high-quality AE-CCSD(T)/cc-pCVQZ energy points. The quantum dynamics was treated within a simple reaction-path hamiltonian model[22] with tunnelling probabilities given by the standard WKB (Wentzel-Kramers-Brillouin) formula in terms of barrier penetration integrals, which we computed numerically from our electronic structure data.

The vibrational 'reaction' mode of **1t** that leads towards **TS2** has a harmonic frequency of $\omega_0 = 1,220\ \mathrm{cm}^{-1}$. The tunnelling lifetime of *trans*-H–C–OH near 0 K is obtained by ascribing a 'collision' energy (ε) equivalent to the zero-point vibrational energy (ZPVE) of the reaction mode ($\omega_0/2$), evaluating the WKB transmission coefficient at this energy, $\kappa(\varepsilon)$, and multiplying by the classical rate (ω_0) at which the reactant hits the barrier[23]. This theoretical analysis yields a half-life of 2.0 h (122 min) for **1t** in its ground vibrational level, implying that the observed $t_{1/2}(\mathrm{H–C–OH}) \approx 2$ h can be fully accounted for by a tunnelling mechanism. The same computational procedure yields a tunnelling half-life for *trans*-H–C–OD of over 1,200 yr, which is also consistent with experiment. Evaluating $\kappa(\varepsilon)$ by fitting the asymmetric Eckart potential[21,24] to the imaginary **TS2** barrier frequency ($\omega^* = 2,174i\ \mathrm{cm}^{-1}$) as well as the ZPVE-corrected reaction energy ($-52.05\ \mathrm{kcal\ mol}^{-1}$) and barrier height ($31.60\ \mathrm{kcal\ mol}^{-1}$) yields qualitatively similar tunnelling lifetimes for both isotopologues of hydroxymethylene.

Pending full-dimensional quantum dynamics computations on a semi-global potential energy surface, we conclude that the disappearance of **1t** is attributable to pure quantum mechanical tunnelling under a barrier in excess of 30 kcal mol^{-1}. The occurrence of such an event near 0 K on a timescale of a few hours is a striking chemical phenomenon with little precedent[25–28].

It has been proposed that **1** may exist in interstellar space and that its reaction with **2** would be a possible source of simple sugars[8]. The properties of hydroxymethylene revealed in our experiments raise considerable problems for the astronomical detection of **1t**, as well as its participation in interstellar chemistry at very low pressures.

That is, molecule **1t** will be inherently unstable at all energies unless it is formed in an almost perfect quantum mechanical stationary state whose vibrational wavefunction is highly localized, despite the propensity of this species, at least in dissipative surroundings, to tunnel to **2** and become trapped there. Extensive theoretical work[29] on the acetylene/vinylidene isomerization suggests that such long-lived hydroxymethylene states may in principle exist *in vacuo*, but populating and characterizing them would certainly be a formidable experimental challenge.

METHODS SUMMARY

Several HVFP matrix isolation experiments were performed to determine the optimal pyrolysis temperature (1,000 °C) for producing **1**. Condensing the decarboxylation products of **3** on a cold window at 11 K in an Ar matrix ultimately achieved a **1**:**2** ratio of 1:5.5. Comparable results were obtained from experiments in Kr, Xe and N_2 matrices and at temperatures above 11 K (compare Supplementary Table 1). In addition to the parent isotopologue **1**, monodeuterated H–C–OD ([D_1]-**1**) was prepared from HC(O)-C(O)OD and was subjected to the same detailed experimental and computational scrutiny.

The electronic structure computations used correlation-consistent families [(aug)-cc-p(C)VXZ] of atomic-orbital basis sets. Most electronic wavefunctions were determined with single-reference coupled-cluster theory, incorporating all single and double excitations (CCSD), and with perturbative inclusion of connected triple excitations [CCSD(T)]. Higher-order correlation effects were evaluated similarly with the CCSDT(Q) method. Optimum geometric structures for all species on the ground-state singlet surface were obtained with all-electron (AE) CCSD(T) theory using the cc-pCVQZ basis set. Final energetics were determined by means of valence focal-point extrapolations[16] with the cc-pVXZ series of basis sets from $X = 2$ through to 6. The valence FPA results were appended with core correlation shifts, as well as one-electron mass-velocity and Darwin relativistic corrections, both computed at the CCSD(T)/cc-pCVQZ level.

For anharmonic vibrational computations, AE-CCSD(T)/cc-pCVQZ complete quartic force fields were evaluated for all minima on the ground-state singlet surface. VBOs for hydroxymethylene were computed with a variational approach called DEWE that constructs a discrete variable representation of the full normal-coordinate Eckart-Watson hamiltonian but handles any internal-coordinate potential function via an analytical transformation[30]. The VBOs in Table 1 were computed from an optimal Simons-Parr-Finlan representation of the AE-CCSD(T)/cc-pCVQZ quartic force field, using sufficient grid points to converge the eigenvalues to better than 0.1 cm^{-1}.

Full Methods and any associated references are available in the online version of the paper at www.nature.com/nature.

1. Bourissou, D., Guerret, O., Gabbaï, F. P. & Bertrand, G. Stable carbenes. *Chem. Rev.* **100**, 39–91 (2000).
2. Nolan, S. P. *N-Heterocyclic Carbenes in Synthesis* (Wiley-VCH, Weinheim, 2006).
3. Kemper, M. J. H., Vandijk, J. M. F. & Buck, H. M. Ab initio calculation on the photochemistry of formaldehyde. The search for a hydroxycarbene intermediate. *J. Am. Chem. Soc.* **100**, 7841–7846 (1978).
4. Lucchese, R. R. & Schaefer, H. F. Metal-carbene complexes and the possible role of hydroxycarbene in formaldehyde laser photochemistry. *J. Am. Chem. Soc.* **100**, 298–299 (1978).
5. Hoffmann, M. R. & Schaefer, H. F. Hydroxycarbene (HCOH) and protonated formaldehyde: Two potentially observable interstellar molecules. *Astrophys. J.* **249**, 563–565 (1981).
6. Reid, D. L., Hernández-Trujillo, J. & Warkentin, J. A theoretical study of hydroxycarbene as a model for the homolysis of oxy- and dioxycarbenes. *J. Phys. Chem. A* **104**, 3398–3405 (2000).
7. Goddard, J. D. & Schaefer, H. F. The photodissociation of formaldehyde: Potential energy surface features. *J. Chem. Phys.* **70**, 5117–5134 (1979).
8. Baly, E. C. C., Heilbron, I. M. & Barker, W. F. CX.—Photocatalysis. Part I. The synthesis of formaldehyde and carbohydrates from carbon dioxide and water. *J. Chem. Soc. Trans.* **119**, 1025–1035 (1921).
9. Sierra, M. A. Di- and polymetallic heteroatom stabilized (Fischer) metal carbene complexes. *Chem. Rev.* **100**, 3591–3637 (2000).
10. Pau, C.-F. & Hehre, W. J. Relative thermochemical stabilities of hydroxymethylene and formaldehyde by ion cyclotron double resonance spectroscopy. *J. Phys. Chem.* **86**, 1252–1253 (1982).
11. Fischer, E. O. & Maasböl, A. On existence of tungsten carbonyl carbene complex. *Angew. Chem. Int. Edn Engl.* **3**, 580–581 (1964).
12. Weiner, B. R. & Rosenfeld, R. N. Pyrolysis of pyruvic acid in the gas phase. A study of the isomerization mechanism of a hydroxycarbene intermediate. *J. Org. Chem.* **48**, 5362–5364 (1983).

13. Rosenfeld, R. N. & Weiner, B. Energy disposal in the photofragmentation of pyruvic acid in the gas phase. *J. Am. Chem. Soc.* **105**, 3485–3488 (1983).

14. Jacox, M. E. The spectroscopy of molecular reaction intermediates trapped in the solid rare gases. *Chem. Soc. Rev.* **31**, 108–115 (2002).

15. Evangelista, F. A., Allen, W. D. & Schaefer, H. F. Coupling term derivation and general implementation of state-specific multireference coupled cluster theories. *J. Chem. Phys.* **127**, 024102 (2007).

16. Császár, A. G., Allen, W. D. & Schaefer, H. F. In pursuit of the *ab initio* limit for conformational energy prototypes. *J. Chem. Phys.* **108**, 9751–9764 (1998).

17. Schreiner, P. R. & Reisenauer, H. P. The ''non-reaction'' of ground-state triplet carbon atoms with water revisited. *ChemPhysChem* **7**, 880–885 (2006).

18. Venkateswarlu, P. & Gordy, W. Methyl alcohol II. Molecular structure. *J. Chem. Phys.* **23**, 1200–1202 (1955).

19. Reisenauer, H. P., Romanski, J., Mloston, G. & Schreiner, P. R. Dimethoxycarbene: Conformational analysis of a reactive intermediate. *Eur. J. Org. Chem.* 4813–4818 (2006).

20. Sodeau, J. R. & Lee, E. K. C. Intermediacy of hydroxymethylene (HCOH) in the low temperature matrix photochemistry of formaldehyde. *Chem. Phys. Lett.* **57**, 71–74 (1978).

21. Miller, W. H. Tunneling corrections to unimolecular rate constants, with application to formaldehyde. *J. Am. Chem. Soc.* **101**, 6810–6814 (1979).

22. Miller, W. H., Handy, N. C. & Adams, J. E. Reaction path Hamiltonian for polyatomic molecules. *J. Chem. Phys.* **72**, 99–112 (1980).

23. Carrington, T. Jr, Hubbard, L. M., Schaefer, H. F. & Miller, W. H. Vinylidene: Potential energy surface and unimolecular reaction dynamics. *J. Chem. Phys.* **80**, 4347–4354 (1984).

24. Johnston, H. S. *Gas Phase Reaction Rate Theory* (Ronald Press, New York, 1966).

25. McMahon, R. J. & Chapman, O. L. Direct spectroscopic observation of intramolecular hydrogen shifts in carbenes. *J. Am. Chem. Soc.* **109**, 683–692 (1987).

26. Zuev, P. S. & Sheridan, R. S. Tunneling in the C–H insertion of a singlet carbene: *tert*-Butylchlorocarbene. *J. Am. Chem. Soc.* **116**, 4123–4124 (1994).

27. Pettersson, M. *et al. Cis → trans* conversion of formic acid by dissipative tunneling in solid rare gases: Influence of environment on the tunneling rate. *J. Chem. Phys.* **117**, 9095–9098 (2002).

28. Maçôas, E. M. S., Khriachtchev, L., Pettersson, M., Fausto, R. & Räsänen, M. Rotational isomerism of acetic acid isolated in rare-gas matrices: Effect of medium and isotopic substitution on IR-induced isomerization quantum yield and *cis → trans* tunneling rate. *J. Chem. Phys.* **121**, 1331–1338 (2004).

29. Zou, S., Bowman, J. M. & Brown, A. Full-dimensionality quantum calculations of acetylene–vinylidene isomerization. *J. Chem. Phys.* **118**, 10012–10023 (2003).

30. Mátyus, E., Czakó, G., Sutcliffe, B. T. & Császár, A. G. Vibrational energy levels with arbitrary potentials using the Eckart-Watson Hamiltonians and the discrete variable representation. *J. Chem. Phys.* **127**, 084102 (2007).

Author Contributions P.R.S. and H.P.R. formulated the initial working hypothesis and provided, analysed and interpreted all experimental data. F.C.P. and A.C.S. performed all the electronic structure computations under the direction of W.D.A. The variational vibrational computations were executed by E.M. under the guidance of A.G.C. and W.D.A. The tunnelling analysis was performed by W.D.A., with input from F.C.P. and A.C.S. The manuscript was primarily written by P.R.S. and W.D.A.

Author Information Reprints and permissions information is available at www.nature.com/reprints. Correspondence and requests for materials should be addressed to P.R.S. (prs@org.chemie.uni-giessen.de) or W.D.A. (wdallen@uga.edu).

METHODS

Matrix isolation studies. The cryostat used for the matrix isolation studies was an APD Cryogenics HC-2 closed-cycle refrigerator system fitted with CsI windows for infrared (IR) and BaF_2 windows for ultraviolet/visible (UV/Vis) measurements. IR spectra were recorded with a Bruker IFS 55 FTIR spectrometer (4,500–300 cm^{-1}, resolution 0.7 cm^{-1}), and UV/Vis spectra were recorded with an Agilent HP 8453 diode-array spectrometer and a JASCO V-670 spectrophotometer. For the combination of HVFP with matrix isolation we used a home-built, water-cooled oven directly connected to the vacuum shroud of the cryostat. The pyrolysis zone consisted of an empty quartz tube (inner diameter 8 mm, length of heating zone 50 mm) resistively heated by a wire. The temperature was controlled by a Ni/CrNi thermocouple. Water-free glyoxylic acid was prepared by heating the commercially available monohydrate (Sigma-Aldrich) under vacuum for several days; monodeuterated glyoxylic acid was obtained by dissolving the monohydrate in D_2O and evaporating to dryness three times. The precursors were evaporated from a heated storage bulb (70–80 °C) into the quartz pyrolysis tube. Immediately after leaving the tube, at a distance of ~50 mm, the pyrolysis products were co-condensed with a large excess of either argon, krypton, xenon, or nitrogen on the surface of the cold matrix window. For irradiations a mercury high-pressure lamp (HBO 200, Osram) with a monochromator (Bausch & Lomb) was used (band width ~10 nm).

Several experiments were performed in order to determine the optimal reaction temperature (1,000 °C). Under these conditions the decarboxylation reactions were not complete, and unreacted precursors were always present in the matrices. Moreover, the main reaction products in the matrix were CO_2, formaldehyde (**2**), and small amounts of CO. The yield of matrix-isolated hydroxymethylene (**1**) compared to formaldehyde was about 20%. By measuring the spectral differences of irradiated and unirradiated matrices, it was possible to elaborate the IR and UV/Vis spectral properties of **1**, despite its low concentration.

The kinetics of the thermal rearrangement of **1** to **2** at 11 K (lowest achievable temperature), 15 K and 20 K were investigated by taking IR spectra every 30 min while keeping the cryostat at the respective temperature and carefully shielding it from all external light sources (compare Supplementary Table 1). Decrease of the two most intense peaks of **1** at ~1,050 and 1,300 cm^{-1} clearly followed first-order kinetics with a half-life of around 2 h in Ar, Kr and Xe, whereas the lifetime of **1** in an N_2 matrix was prolonged by a factor larger than three. The bands of $[D_1]$-**1t** did not change under identical conditions for extended periods of time.

Electronic structure computations. The Supplementary Information contains extensive details of the electronic structure computations. The AE-CCSD(T)/cc-pCVQZ optimum geometric structures for all species on the ground-state singlet surface are depicted in Supplementary Fig. 1, and corresponding atomic cartesian coordinates are given in Supplementary Tables 2 and 3. All of the explicitly computed electronic energies entering into the subsequent focal-point analyses are listed in Supplementary Table 4. The focal-point extrapolations, with auxiliary core correlation, relativistic, and ZPVE terms, are laid out in Supplementary Table 5 for the seven relative energies pinpointed in this study. Supplementary Table 6 provides a succinct collection of the final FPA results. Our FPA procedures have been described in earlier publications[16,31–34] and validated on a large number of chemical systems. For completeness, we provide references detailing the cc-pVXZ ($X = 2$–6)[35] and cc-pCVQZ[36] basis sets, our relativistic methods[37–39], and the recently formulated CCSDT(Q) scheme for incorporating connected quadruple excitations into coupled cluster computations[40,41].

The first open-shell singlet excited electronic state (S_1) of H–C–OH was investigated by our recently developed multireference coupled cluster (Mk-MRCCSD) methods[15,42]. For planar geometries, the S_1 state is of $^1A''$ symmetry, arising from the $7a' \rightarrow 2a''$ molecular orbital excitation. The reference determinants for the Mk-MRCCSD computations included all possible distributions of two electrons in the ($7a'$, $2a''$) HOMO/LUMO active space. For planar geometries only two references are of the correct symmetry, but four references must be incorporated when the S_1 state twists out of plane. The optimum (twisted, C_1) structure of the S_1 state, as well as the planar transition state for internal rotation, is shown in Supplementary Fig. 2, as given by our four-reference, all-electron Mk-MRCCSD computations with the aug-cc-pCVTZ basis set. Comparative structures for the ground-state singlet (S_0) and analogous triplet (T_1) states are also given in Supplementary Fig. 2. Cartesian coordinates of the Mk-MRCCSD optimized structures appear in Supplementary Table 7. Supplementary Table 5 gives the total energies involved in our Mk-MRCCSD determination of the vertical and adiabatic excitation energies for the S_1 state. All multireference coupled cluster computations for the S_1 state were carried out using ROHF orbitals optimized on the corresponding triplet state (T_1).

Vibrational computations and tunnelling analysis. Anharmonic ZPVEs of all minima on the ground-state singlet surface were computed by applying vibrational perturbation theory (VPT2)[43–48] to our complete AE-CCSD(T)/cc-pCVQZ quartic force fields, including the G_0 terms[49]. ZPVEs of all transition states were evaluated from harmonic frequencies at the AE-CCSD(T)/cc-pCVQZ level. The quartic force fields were determined from a grid of tightly-converged energy points (263 in the case of **1t**) using established finite-difference techniques[50]. The methodology is implemented in INTDIF2005, which is an abstract program written by W.D.A. for Mathematica to perform general numerical differentiations to high orders of electronic structure data.

For the variational vibrational computations, the potential energy surfaces of the *trans* conformations of H–C–OH and H–C–OD were constructed by transforming the AE-CCSD(T)/cc-pCVQZ quartic force fields to an optimal SPF coordinate representation[51]. The final variational procedure used 531,441 grid points to build the vibrational hamiltonian matrix, which allowed convergence of the eigenvalues to better than 0.1 cm^{-1}. To give a quantitative interpretation of the computed vibrational levels, overlaps of the numerically exact wavefunctions were evaluated over multidimensional normal-mode harmonic oscillator basis functions. The squares of these coefficients comprise the normal mode distributions (NMDs) that describe the vibrational states in Table 1 of the text. Convergence of the NMDs presented in Table 1 is better than 1%.

Our tunnelling analysis employed IRPs[52] and mathematical algorithms[53] for generating them that are widely employed in theoretical chemistry. The application of a reaction path hamiltonian along an IRP requires the computation of vibrational frequencies for modes orthogonal to the path, a task which demands attention to numerous subtle issues[54]. The WKB method[55,56] for evaluating transmission probabilities through a potential energy barrier in terms of barrier penetration integrals is a classic theory that has long been applied to isomerization problems[57].

31. Allen, W. D., East, A. L. L. & Császár, A. G. in *Structures and Conformations of Non-Rigid Molecules* (eds Laane, J., Dakkouri, M., van der Veken, B. & Oberhammer, H.) 343–373 (NATO ASI Series C, Kluwer, Dordrecht, 1993).
32. Császár, A. G. *et al.* in *Spectroscopy from Space* (eds Demaison, J., Sarka, K. & Cohen, E. A.) 317–339 (NATO Science Series II, Vol. 20, Kluwer, Dordrecht, 2001).
33. Schuurman, M. S., Muir, S. R., Allen, W. D. & Schaefer, H. F. Toward subchemical accuracy in computational thermochemistry: Focal point analysis of the heat of formation of NCO and [H,N,C,O] isomers. *J. Chem. Phys.* **120**, 11586–11599 (2004).
34. Gonzales, J. M. *et al.* Definitive ab initio studies of model S_N2 reactions $CH_3X + F^-$ (X = F, Cl, CN, OH, SH, NH_2, PH_2). *Chem. Eur. J.* **9**, 2173–2192 (2003).
35. Dunning, T. H. Jr. Gaussian basis sets for use in correlated molecular calculations. I. The atoms boron through neon and hydrogen. *J. Chem. Phys.* **90**, 1007–1023 (1989).
36. Woon, D. E. & Dunning, T. H. Jr. Gaussian basis sets for use in correlated molecular calculations. V. Core-valence basis sets for boron through neon. *J. Chem. Phys.* **103**, 4572–4585 (1995).
37. Perera, A. S. & Bartlett, R. J. Relativistic effects at the correlated level. An application to interhalogens. *Chem. Phys. Lett.* **216**, 606–612 (1993).
38. Balasubramanian, K. *Relativistic Effects in Chemistry* Part A, *Theory and Techniques* (Wiley, New York, 1997).
39. Tarczay, G., Császár, A. G., Klopper, W. & Quiney, H. M. Anatomy of relativistic energy corrections in light molecular systems. *Mol. Phys.* **99**, 1769–1794 (2001).
40. Bomble, Y. J., Stanton, J. F., Kállay, M. & Gauss, J. Coupled-cluster methods including noniterative corrections for quadruple excitations. *J. Chem. Phys.* **123**, 054101 (2005).
41. Kállay, M. & Gauss, J. Approximate treatment of higher excitations in coupled-cluster theory. *J. Chem. Phys.* **123**, 214105 (2005).
42. Evangelista, F. A., Allen, W. D. & Schaefer, H. F. High-order excitations in state-universal and state-specific multireference coupled cluster theories: Model systems. *J. Chem. Phys.* **125**, 154113 (2006).
43. Watson, J. K. G. in *Vibrational Spectra and Structure*, Vol. 6 (ed. Durig, J. R.) 1–89 (Elsevier, New York and Amsterdam, 1977).
44. Mills, I. M. in *Molecular Spectroscopy: Modern Research* (eds Rao, K. N. & Mathews, C. W.) 1–115 (Academic, New York, 1972).
45. Papoušek, D. & Aliev, M. R. *Molecular Vibrational-Rotational Spectra* (Elsevier, Amsterdam, 1982).
46. Nielsen, H. H. The vibration-rotation energies of molecules. *Rev. Mod. Phys.* **23**, 90–136 (1951).
47. Clabo, D. A. Jr, Allen, W. D., Remington, R. B., Yamaguchi, Y. & Schaefer, H. F. A systematic study of molecular vibrational anharmonicity and vibration-rotation interaction by self-consistent-field higher-derivative methods. Asymmetric top molecules. *Chem. Phys.* **123**, 187–239 (1988).
48. Allen, W. D. *et al.* A systematic study of molecular vibrational anharmonicity and vibration-rotation interaction by self-consistent-field higher-derivative methods. Linear polyatomic molecules. *Chem. Phys.* **145**, 427–466 (1990).
49. Schuurman, M. S., Allen, W. D. & Schaefer, H. F. The *ab initio* limit quartic force field of BH_3. *J. Comput. Chem.* **26**, 1106–1112 (2005).
50. DeKock, R. L. *et al.* The electronic structure and vibrational spectrum of *trans*-HNOO. *J. Phys. Chem. A* **108**, 2893–2903 (2004).

51. Czakó, G., Furtenbacher, T., Császár, A. G. & Szalay, V. Variational vibrational calculations using high-order anharmonic force fields. *Mol. Phys.* **102,** 2411–2423 (2004).

52. Fukui, K. A formulation of the reaction coordinate. *J. Phys. Chem.* **74,** 4161–4163 (1970).

53. Gonzales, C. & Schlegel, H. B. Reaction path following in mass-weighted internal coordinates. *J. Phys. Chem.* **94,** 5523–5527 (1990).

54. Allen, W. D., Bodi, A., Szalay, V. & Császár, A. G. Adiabatic approximations to internal rotation. *J. Chem. Phys.* **124,** 224310 (2006).

55. Liboff, R. L. *Introductory Quantum Mechanics* (Addison-Wesley, Reading, Massachusetts, 2003).

56. Razavy, M. *Quantum Theory of Tunneling* (World Scientific, Singapore, 2003).

57. Gray, S. K., Miller, W. H., Yamaguchi, Y. & Schaefer, H. F. Reaction path Hamiltonian: Tunneling effects in the unimolecular isomerization HNC → HCN. *J. Chem. Phys.* **73,** 2733–2739 (1980).